International Journal of Thermophysics, Vol. 19, No. 5, 1998

The Static Dielectric Constant of Liquid Water Between 274 and 418 K Near the Saturated Vapor Pressure

J. Hamelin,[1] J. B. Mehl,[1,2] and M. R. Moldover[1,3]

Received January 22, 1998

The complex dielectric constant (relative electric permittivity) $\varepsilon_r = \varepsilon' - i\varepsilon''$ of liquid water was redetermined in the temperature range $0°C < t < 145°C$ at pressures less than 440 kPa. In this work, ε_r was deduced from measurements of the resonant frequencies f_α of a novel, re-entrant, two-mode, radio-frequency resonator. The frequencies ranged from 23 to 84 MHz and were well within the low-frequency limit for ε' because $(2\pi f_\alpha \tau_{max})^2 < 5 \times 10^{-5}$ where $\tau_{max} = 1.8 \times 10^{-11}$ s is the maximum relaxation time of water under the conditions studied. The data for ε' for two water samples differing in conductivity by a factor of 3.6 and for the two resonant modes differing in frequency by a factor of 2.6 were simultaneously fit by the polynomial function $\varepsilon'(t) = 87.9144 - 0.404399t + 9.58726 \times 10^{-4}t^2 - 1.32802 \times 10^{-6}t^3$ with a remarkably small residual standard deviation of 0.0055. The present data are consistent with previously published data; however, they are more precise and internally consistent. The present apparatus was also tested with cyclohexane and yielded the values $\varepsilon'(t) = 2.0551 - 0.00156t$ for $20°C < t < 30°C$, in excellent agreement with previously published values.

KEY WORDS: cyclohexane; dielectric constant; re-entrant radio-frequency resonator; relative permittivity; static dielectric constant; water.

1. INTRODUCTION

A recently published database [1] lists 26 sources of data for the real part of the "static" dielectric constant (relative permittivity) ε' of liquid water at

[1] Physical and Chemical Properties Division, National Institute of Standards and Technology, Gaithersburg, Maryland 20899, U.S.A.

[2] Physics Department, University of Delaware, Newark, Delaware 19716, U.S.A.

[3] To whom correspondence should be addressed.

0195-928X/98/0900-1359$15.00/0

temperatures below its normal boiling point. The compilers of the database noted that "discrepancies exist between two groups of the data sets that lead to appreciable uncertainty in the temperature derivative of the dielectric constant in this range" [2]. They were motivated to make new measurements in the range 273 to 373 K to resolve discrepancies and were sucessful below 340 K. However, above 340 K, their results for ε' from two independent audio-frequency methods (LCR meter and a transformer bridge) diverged until they differed by 0.5% near 373 K. This divergence propagated into an uncertainty of 2.8% in the value of $(\partial\varepsilon'/\partial T)_p$ at 373 K, despite the very extensive and careful measurements. As displayed in Fig. 1, the present measurements that were made in the radio-frequency range agree well with the transformer bridge results in Ref. 2 and are consistent

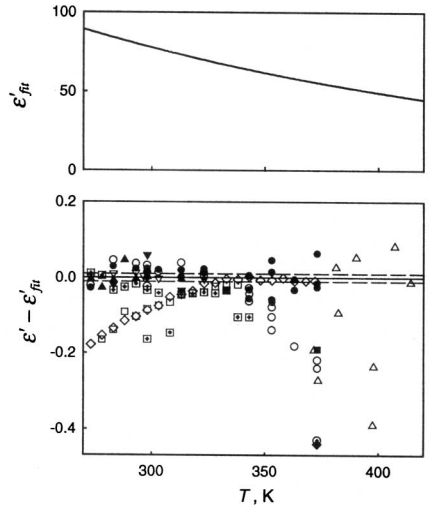

Fig. 1. Top: Eq. (1), the temperature dependence of the real part of the relative dielectric permeability of water. Bottom: Deviations of the literature data from Eq. (1). The dashed lines span $\pm 2s$, where $s = 0.0055$ is the standard deviation of the fit to our data for both modes with Sample A and with Sample B. Data sources: ○ [2], LCR meter; ● [2], transformer bridge; △ [11]; ◇ [12]; ▼ [13]; ⊞ [14]; □ [15]; ■ [16]; ▲ [17]; ▽ [18]; ◆ [19]; ⊕ [20].

with some of the other work in the database given in Ref. 1. The base line in Fig. 1 is the polynomial function of the Celsius temperature t

$$\varepsilon'(t) = 87.9144 - 0.404399t + 9.58726 \times 10^{-4}t^2 - 1.32802 \times 10^{-6}t^3 \qquad 0°\text{C} < t < 145°\text{C} \tag{1}$$

which represents our data with a residual standard deviation $s = 0.0055$.

The present measurements yield values of $(\partial\varepsilon'/\partial T)_p$ with a residual standard deviation of 0.0018 K^{-1} in the temperature range 274 to 418 K. (The derivative was computed from a linear fit to groups of successive groups of data points spanning intervals of 20 to 30 K.) Thus, present values of ε' and $(\partial\varepsilon'/\partial T)_p$ appear to be a factor of 5 more precise than those in Ref. 1. We hope that the present values of ε' have smaller "bias" or systematic errors than other previous values. To explore this possibility, we now discuss tests for systematic errors.

In this work, both the real and the imaginary parts of $\varepsilon_r = \varepsilon' - i\varepsilon''$ were deduced from measurements of the resonant frequencies f_α of a novel, reentrant, two-mode, radio-frequency resonator. A brief description of the resonator is provided below. A more complete description of the resonator, a model for its equivalent circuit, and the methods for determining ε_r from its frequency response have been published elsewhere [3]. When the resonator was filled with a dielectric fluid, the resonant modes occurred near the frequencies $f_{\text{low}} = 216/\sqrt{\varepsilon'}$ MHz and $f_{\text{high}} = 566/\sqrt{\varepsilon'}$ MHz. Each mode was used to determine independent values of ε' (denoted $\varepsilon'_{\text{low}}$ and $\varepsilon'_{\text{high}}$) for the same sample under the same physical conditions. This redundancy provided one test for systematic errors. A second test for systematic errors used the measurements of ε' from water samples of differing purity and therefore of differing conductivity. At 23°C and 290 Hz, Sample A had a specific conductivity of 109 $\mu\text{S} \cdot \text{m}^{-1}$; that of Sample B was 30 $\mu\text{S} \cdot \text{m}^{-1}$. The effects of changing frequency and sample conductivity are summarized in Fig. 2 which displays the present data for ε' as deviations from Eq. (1). Figure 2 shows that changing the frequency by a factor of 2.6 or changing the conductivity by a factor of 3.6 produce changes in ε' on the order of 0.01%. These changes are remarkably small when plotted on a scale that displays the results from various laboratories. (See Fig. 1.)

In a final search for systematic errors, the present apparatus was used to measure ε_r of the nonpolar, nonconducting liquid, cyclohexane. The results for ε' from both modes of the resonator are in excellent agreement with previously published values, as shown in Table I. The present results are represented by the expression

$$\varepsilon'(t) = 2.0551 - 0.00156t \qquad 20°\text{C} < t < 30°\text{C} \tag{2}$$

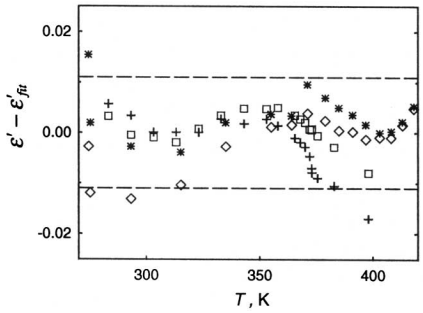

Fig. 2. Differences between measured values of ε' and Eq. (1). The dashed lines are drawn at $\pm 2s$ where $s = 0.0055$ is the residual standard deviation between the measurements and Eq. (1). Key: □ Sample A, high mode; + Sample A, low mode; ◇ Sample B, high mode; * Sample B, low mode.

with a residual standard deviation $s = 0.00012$. The deviations are not random; the three values of ε' at 150 MHz fall 0.0001 below Eq. (2) and the three values of ε' at 400 MHz fall 0.0001 above Eq. (2). When the residual standard deviations are scaled by typical values of ε', the result for cyclohexane ($s/\varepsilon' = 0.00012/2 = 6 \times 10^{-5}$) is comparable to that for water ($s/\varepsilon' = 0.0055/70 = 8 \times 10^{-5}$).

The present measurements differ from previous radio-frequency resonance measurements of ε' in two key respects. First, in earlier work (for example, in Ref. 4), the resonance frequencies were determined by locating the frequencies of maximum power transmission through the resonator. In the present work, $\varepsilon_r = \varepsilon' - i\varepsilon''$ was determined by fitting a complex Lorentzian function to both the real and the imaginary parts of the frequency response of the resonator within the interval $f_\alpha \pm 2g_\alpha$ centered about each resonance frequency. (The subscript "α" stands for either "high"

Table I. Dielectric Constant of Cyclohexane near Ambient Conditions at $p = 99$ kPa

	293.15 K	298.15 K	303.15 K
Low mode	2.0238	2.0160	2.0082
High mode	2.0240	2.0162	2.0084
Ref. 21		2.01714	
Ref. 22	2.0240		2.0119
Ref. 23	2.0228	2.0150	2.0077

or "low;" f_α is a resonance frequency and g_α is the half-width of the resonance at $1/\sqrt{2}$ of its maximum amplitude.) In contrast with prior work and as discussed in Section 3.2 below, the present fitting procedure accounts for corrections to the resonance frequencies on the order of $2g_\alpha/f_\alpha = 1/Q$. Second, in prior work, the resonances were wider than expected considering the construction of the resonator and considering the coupling of the resonator to the external circuit. In contrast with prior work, the widths of the present resonances are completely understood. When the widths of resonances are not fully understood, systematic errors may result.

In radio frequency resonators, including the present one, the conductivity of water σ_{rf} contributes a term $1/Q_w = \varepsilon''/\varepsilon' = 2\pi\sigma_{rf}f/\varepsilon'$ to $1/Q$. When we used sufficiently impure water so that $1/Q \gtrsim 0.02$, the frequency responses of the resonator were inconsistent with Lorentzian functions. Under the same circumstances, the apparent values of ε' deduced from the two modes were inconsistent. Both inconsistencies signaled that the data for very impure water were outside the range where the present resonator is well understood. Thus, the data for which $1/Q \gtrsim 0.02$ were not used in the final determination of ε'. If we had used only a single resonance and determined ε' from the frequency of maximum power transmission, we might not have detected the failure of the model used to determine ε' from the data.

2. TWO-MODE RE-ENTRANT RESONATOR

The two-mode re-entrant resonator used in this work was developed for dielectric measurements with fluids such as water. Its design and construction were described in Ref. 3. This design evolved from a single-mode resonator described in Ref. 5. In the present design, the two resonance frequencies are sufficiently high that electrode polarization phenomena are negligible, yet they are not so high that the frequency dependence of ε' enters into the analysis of the data. (If the frequency dependence of ε' were to be studied, a similar resonator could be designed with several modes resonant at higher frequencies.)

The resonance frequency data were analyzed with the simple lumped-component equivalent circuit shown in Fig. 3. This circuit accounts for the coupling of the resonator to the external instruments and for the loading of the resonator by these instruments. Furthermore, this circuit can easily be generalized for a resonator with three or more modes. Measurements of the complex resonance frequencies $\mathbf{F}_\alpha^0 = f_\alpha^0 + ig_\alpha^0$ of the evacuated resonator were used to determine combinations of component values for the equivalent circuit. Careful measurements of the resonator's dimensions were not required. The resonator's dilation with pressure was accounted for by

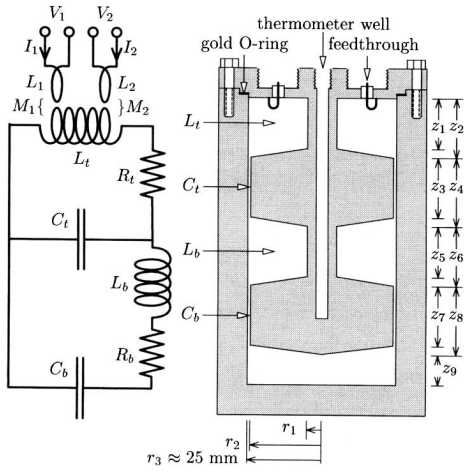

Fig. 3. Two-mode re-entrant radio-frequency resonator and equivalent circuit. The dimensions z_1 through z_9 and r_1 through r_3, in mm, are: 17.19, 20.07, 20.12, 23.15, 16.98, 19.87, 19.99, 23.01, 10.7, and 5.015, 23.98, 24.95, respectively. The approximate values of the components in vacuum are: $L_t = 5.88$ nH, $C_t = 33.5$ pF, $L_b = 6.19$ nH, $C_b = 35.2$ pF, $M_1 = M_2 = 0.17$ nH, $L_1 = L_2 = 9.6$ nH and the effective resistances R_t and R_b are 0.008Ω at f_{low} and 0.0058Ω at f_{high}.

measuring f_α in helium as a function of pressure and correcting the results for the small dielectric polarizability of helium.

In essence, the resonator method for determining ε_r is to measure the complex resonance frequencies of the evacuated resonator $\mathbf{F}_\alpha^0$ and of the water filled resonator $\mathbf{F}_\alpha$ and to use the relation

$$\varepsilon_r = (\mathbf{F}_\alpha^0/\mathbf{F}_\alpha)^2 \tag{3}$$

Equation (3) would be exact if the spatial distribution of the electric and magnetic fields within the resonator were identical in the empty and filled configurations. The most important correction to Eq. (3) results from the penetration of the magnetic field into the metal surfaces bounding the resonator. The penetration depth $\delta_\alpha = 1/\sqrt{\pi f_\alpha \mu' \sigma'}$, where μ' and σ' are the magnetic permeability and electric conductivity of the metal surface, respectively. The penetration increases the half-widths of the resonances by an amount g_s and decreases the resonance frequencies by

this same amount. For our gold-plated resonator, $\mu' \approx \mu_0$ and $\sigma' = (4.955 \times 10^7/[1 + 0.00407t])\ \mathrm{S \cdot m^{-1}}$, independent of the frequency. The penetration depths are $\delta_{\mathrm{high}} \approx 3(\varepsilon')^{1/4}\,\mu\mathrm{m}$ and $\delta_{\mathrm{low}} \approx 5(\varepsilon')^{1/4}\,\mu\mathrm{m}$. The fractional corrections to Eq. (3) are of the order of

$$g_{s\alpha}/f_\alpha \sim \delta_\alpha/z \sim 0.001 \tag{4}$$

where $z \sim 5$ mm is a typical length of a component of the resonator. These corrections had to be made carefully because δ_α approximately triples when the resonance frequencies are reduced by filling the resonator with water. (Before plating the resonator with gold, $g_{s\alpha}/f_\alpha$ was larger than expected and had a complicated frequency dependence, presumably because μ' of stainless steel is much greater than 1 and μ' of steels varies with temperature, frequency, and heat treatment in a complicated way.)

A working equation for ε_r that accounts for the penetration lengths δ_α was derived in Ref. 3:

$$\varepsilon_r = \left(\frac{\mathbf{F}_\alpha^0}{\mathbf{F}_\alpha}\right)^2 \frac{1 + (-1+i)\,\varepsilon_r (f_\alpha/f_\alpha^0)^{3/2}\,(2g_\alpha^0/f_\alpha^0)}{1 + (-1+i)(2g_\alpha^0/f_\alpha^0)} \tag{5}$$

Equation (5) is significantly more accurate than Eq. (3). It was derived using the equivalent circuit components L_t, C_t, L_b, C_b, R_t, and R_b displayed in Fig. 3. However, the results are expressed in terms of the electrically measured quantities for the evacuated resonator ($\mathbf{F}_\alpha^0 = f_\alpha^0 + ig_\alpha^0$) and the same quantities measured for the water-filled resonator ($\mathbf{F}_\alpha = f_\alpha + ig_\alpha$). Implicitly, Eqs. (3) and (5) assume that the dimensions of the resonator are not changed when water replaces vacuum in its interior. Thus, Eq. (5) can be used only after making a very small correction to $\mathbf{F}_\alpha$ for the resonator's dilation under pressure, and only if $\mathbf{F}_\alpha$ and $\mathbf{F}_\alpha^0$ are measured at nearly the same temperature.

In future work, a resonator will be constructed such that its coupling to the external circuit can be neglected. Unfortunately, this was not the case for the present resonator. Thus, we used a slightly more complicated working equation [3]

$$\varepsilon_r = \left(\frac{\mathbf{F}_\alpha^0}{\mathbf{F}_\alpha}\right)^2 \frac{1 + (-1+i)\,\varepsilon_r (f_\alpha/f_\alpha^0)^{3/2}\,(2g_\alpha^0/f_\alpha^0) + i/Q_e + D_\alpha}{1 + (-1+i)(2g_\alpha^0/f_\alpha^0) + i/Q_e^0 + D_\alpha^0} \tag{6}$$

that also accounts for the components M_1, M_2, L_1, and L_2 in Fig. 3. The term $1/Q_e^0$ measured at 293 K is 1.3×10^{-4} for f_{high} and 1.5×10^{-4} for f_{low}. This term is purely dissipative for ε_r real and its magnitude decreases rapidly with frequency, becoming only 2×10^{-5} for both modes in the

water-filled resonator. For vacuum measurements, $D^0_{high} \approx 75 \times 10^{-6}$ and $D^0_{low} \approx 32 \times 10^{-6}$. For water measurements, both D_{high} and D_{low} are less than 2×10^{-6}.

In summary, the present determination of ε_r using the reentrant resonator relies primarily on the measurements of frequencies and half-widths of the evacuated and water-filled resonator. Small corrections [Q's and D's in Eq. (6)] are applied to account for the coupling to external circuitry. These corrections rely on approximate values for the equivalent-circuit components L_t, C_t, M_1, etc. which were determined from simple dimensional measurements [3]. The gold plating was required so that the frequency dependence g_α would be predictable. An incidental advantage of the plating was to make g_α small which leads to large signal-to-noise ratios.

For completeness, we mention that liquid water is diamagnetic with a relative magnetic permeability $\mu_r = \mu/\mu_0 = 1 - 9.1 \times 10^{-6}$ near ambient conditions. Thus, in Eqs. (3) to (6), the quantity ε_r should be replaced by the product $\varepsilon_r \mu_r$; however, the difference between μ_r and 1 is small enough to be neglected in the present work.

3. EXPERIMENTAL MATERIALS AND TECHNIQUES

3.1. The Re-Entrant Resonator

As shown in Fig. 3, the re-entrant resonator was machined from two pieces of 316 stainless steel that were bolted together and sealed with a gold O-ring to form a pressure vessel. A fill line was welded to the upper piece and was used to load fluid samples and to evacuate the resonator. The inner surfaces of the resonator were electroplated with gold to a thickness of at least 30 μm. The plating with a non-magnetic metal was required to insure that the microwave penetration length had a predictable frequency dependence.

The two electrical feedthroughs were made of gold-plated Kovar,[4] insulated with glass, and manufactured by Northeast Electronics Corp.[4] The feedthroughs were soldered into the upper part of the resonator. Two semi-rigid coaxial cables led from the feedthroughs to the network analyzer that was used to measure the resonance frequencies. Inside the resonator, the center conductors of the feedthroughs were bent into U-shapes forming

[4] To describe materials and experimental procedures adequately, it is occasionally necessary to identify commercial products by the manufacturer's name or label. In no instance does such identification imply endorsement by the National Institute of Standards and Technology, nor does it imply that the particular product or equipment is necessarily the best available for the purpose.

semi-circular coupling loops with straight extensions. The center conductors had a diameter of 0.66 mm, the coupling loops had a mean diameter of 5.0 mm, and the straight extensions were approximately 2.6 mm long. The coupling loops were oriented at 45° with respect to a plane including the axis of the resonator and the center line of the feedthrough. Additional details are provided in Ref. 3.

3.2. Resonance Frequencies and Half-Widths

A network analyzer (Hewlett-Packard,[4] Model 8753B) was used to measure the "scattering matrix" parameter $\mathbf{S}_{21}$ for the resonator. For properly terminated transmission lines, $\mathbf{S}_{21}$ equals the vector ratio of the transmitted voltage to the incident voltage. The data were acquired in the interval $f_\alpha \pm 2g_\alpha$ centered about each resonance frequency and were then fit to the expected Lorentzian function

$$\mathbf{S}_{21}(f) = \frac{\mathbf{A}f}{f^2 - \mathbf{F}_\alpha^2} + \mathbf{B} + \mathbf{C}(f - \bar{f}) \tag{7}$$

where $\bar{f}$ is any fixed frequency near f_α. The fitting parameters **A**, **B**, **C**, and $\mathbf{F}_\alpha$ are all complex numbers; thus, eight parameters were used. The procedure for fitting complex Lorentzian functions of the frequency has been used in our laboratory for more than two decades in the course of high-precision studies of gas-filled acoustic resonators [6]. When resonances are well-separated in frequency, the fitting procedure can determine the real and imaginary parts of $\mathbf{F}_\alpha$ with a fractional uncertainty on the order of $(2g_\alpha/f_\alpha)/(s/n)$ where (s/n) is the appropriate signal-to-noise ratio. Moreover, this procedure is effective in eliminating certain systematic errors, including the effects of background signals and crosstalk superimposed on the resonance data, to the extent that they are linear functions of the frequency. In the present work, signal-to-noise was not a limitation. Instead, the theoretical model for $\mathbf{S}_{21}$ is systematically incorrect for resonances with large values of $1/Q$ in a way that is not understood (Section 5.3). Therefore, data with $1/Q \geqslant 0.02$ were not used.

Near the resonances, Eq. (7) is an accurate approximation to a more exact expression for $\mathbf{S}_{21}$ based on the circuit model [3]. The quality of the approximation was tested by numerically generating synthesized data from the more exact expression for $\mathbf{S}_{21}$ and fitting them. Equation (7) led to values of f_α that were approximately a fraction $1/(8Q^2) = g^2/(2f^2)$ larger than the values used in the synthetic data. For most of the data, this is a small effect. The frequencies listed in Tables II and III have not been

Table II. Data and Results for Three Water Samples

T (K)	P (kPa)	f_{low} (MHz)	g_{low} (MHz)	ε'_{low}	σ_{low} (mS·m^{-1})	f_{high} (MHz)	g_{high} (MHz)	ε'_{high}	σ_{low} (mS·m^{-1})
				Sample A					
273.59[a]	100	23.0692	0.0924	87.728	0.33	60.4647	0.2496	87.712	0.42
283.15	100	23.5738	0.1031	83.967	0.37	61.7943	0.2165	83.970	0.55
293.13	100	24.1158	0.1169	80.207	0.70	63.2158	0.2263	80.210	0.69
303.12	100	24.6702	0.1348	76.619	0.66	64.6687	0.2041	76.620	0.83
313.10	100	25.2346	0.1613	73.202	1.07	66.1494	0.2428	73.205	1.02
323.13	99	25.8140	0.1853	69.932	1.13	67.6674	0.2447	69.931	1.17
333.05	100	26.3977	0.2163	66.850	1.43	69.1983	0.2828	66.849	1.36
343.22	99	27.0095	0.2398	63.834	1.51	70.8020	0.2962	63.831	1.46
353.11	100	27.6166	0.2835	61.035	1.81	72.3953	0.3457	61.033	1.70
358.15	99	27.9315	0.2874	59.658	1.76	73.2203	0.3421	59.654	1.68
403.13	275	30.9119	0.2658	48.633	1.25	81.0361	0.3182	48.632	1.36
362.06[a]	99	28.1838	0.3012	58.602	1.84	73.8722	0.3580	58.583	1.74
363.11[a]	100	28.2499	0.3071	58.323	1.90	74.0468	0.3671	58.307	1.77
365.63	100	28.4055	0.3176	57.668	1.94	74.4630	0.3762	57.664	1.82
368.05	100	28.5607	0.3279	57.038	1.98	74.8701	0.3853	57.034	1.87
370.13	101	28.6947	0.3350	56.503	2.01	75.2215	0.3919	56.498	1.89
372.20	101	28.8288	0.3421	55.974	2.03	75.5732	0.3986	55.969	1.92
373.04	148	28.8831	0.3834	55.761	2.26	75.7156	0.4366	55.754	2.17
373.16	250	28.8906	0.3840	55.731	2.28	75.7349	0.4387	55.723	2.17
375.62	150	29.0509	0.4107	55.113	2.28	76.1565	0.4429	55.104	2.31
383.01	200	29.5380	0.4315	53.295	2.36	77.4346	0.4678	53.287	2.35
398.06	251	30.5592	0.4930	49.764	2.58	80.1134	0.5339	49.755	2.53
				Sample B					
274.35	100	23.1041	0.0742	87.446	0.25	60.5677	0.2445	87.428	0.31
275.11	102	23.1459	0.0590	87.128	0.11	60.6759	0.2241	87.114	0.15
293.13	102	24.1171	0.0559	80.203	0.14	63.2218	0.1633	80.192	0.14
315.14	102	25.3529	0.0629	72.521	0.22	66.4608	0.1396	72.514	0.25
335.11	102	26.5219	0.0791	66.224	0.33	69.5252	0.1427	66.219	0.40
355.11	102	27.7428	0.1199	60.482	0.58	72.7255	0.1841	60.479	0.78
364.18	102	28.3143	0.1360	58.047	0.66	74.2235	0.1951	58.045	0.78
371.20	102	28.7625	0.1511	56.239	0.74	75.4013	0.2073	56.233	0.85
379.03	129	29.2742	0.1706	54.275	0.83	76.7426	0.2241	54.270	0.93
385.11	160	29.6781	0.1841	52.796	0.88	77.8019	0.2363	52.792	0.98
391.14	191	30.0847	0.1999	51.368	0.95	78.8675	0.2506	51.364	1.04
396.93	229	30.4803	0.2443	50.032	1.17	79.9055	0.3104	50.028	1.35
403.13	275	30.9119	0.2658	48.633	1.25	81.0361	0.3182	48.632	1.36
408.17	317	31.2682	0.2789	47.522	1.29	81.9708	0.3279	47.520	1.38
413.17	366	31.6260	0.2910	46.444	1.32	82.9082	0.3432	46.444	1.43
418.21	419	31.9926	0.3059	45.377	1.36	83.8698	0.3550	45.377	1.46

[a] Data affected by bubbles; not fitted.

Table II. *(Continued)*

T (K)	P (kPa)	f_{low} (MHz)	g_{low} (MHz)	ε'_{low}	σ_{low} (mS·m^{-1})	f_{high} (MHz)	g_{high} (MHz)	ε'_{high}	σ_{low} (mS·m^{-1})
					Sample C				
278.16	100	23.3056	0.2913	85.910	2.34	61.0958	0.4687	85.906	2.61
288.12	100	23.8406	0.3689	82.058	2.98	62.4988	0.5254	82.064	3.32
298.08	100	24.3868	0.4806	78.376	3.85	63.9338	0.6104	78.392	4.13
308.16	100	24.9507	0.6060	74.821	4.74	65.4160	0.7123	74.852	4.95
318.16	100	25.5159	0.7774	71.475	5.90	66.9167	0.8667	71.502	6.06
328.12	101	26.0956	0.9424	68.263	6.90	68.4371	1.0025	68.332	6.90
338.11	101	26.6910	1.1183	65.174	7.86	69.9976	1.1462	65.291	7.69
348.10	101	27.2928	1.3707	62.219	9.26	71.5898	1.3379	62.390	8.72
358.12	101	27.9145	1.5782	59.382	10.22	73.2193	1.5354	59.614	9.67
368.09	102	28.5434	1.7569	56.710	10.90	74.8935	1.6665	56.954	10.09
379.91	150	29.3107	2.0524	53.642	12.08	76.9302	1.8687	53.947	10.79
388.21	198	29.8631	2.2744	51.570	12.90	78.3993	2.0326	51.921	11.34

corrected for this effect; however, the tabulated values of f_α were multiplied by the factor $[1-g_\alpha^2/(2f_\alpha^2)]$ prior to determining ε'_{high} and ε'_{low} from Eq. (6).

3.3. Water Samples

Three water samples denoted A, B, and C were used for the measurements of ε_r. Each sample was of high purity but had different ionic content. Sample A was purchased from Fluka Chemika.[4] The manufacturer stated that it had a specific conductivity of $5.6\,\mu S \cdot m^{-1}$ during the production process and less than 0.001% residues after evaporation. Sample C was taken from the same container; however, we added a small quantity (approximately, $0.1\ g \cdot dm^{-3}$) of NaCl to it in order to increase its conductivity by a factor of 5. Using Eq. (6.28) in Ref. 10 one may estimate that the NaCl decreases ε' by less than 0.0001, a negligible amount. Sample B was demineralized water filtered through a Barnstead E-pure[4] system.

Table III. Data and Results for Cyclohexane at 99 kPa

T (K)	f_{low} (MHz)	g_{low} (MHz)	ε'_{low}	f_{high} (MHz)	g_{high} (MHz)	ε'_{high}
293.143	151.27870	0.07136	2.0238	397.16546	0.11365	2.0240
298.124	151.55762	0.07202	2.0161	397.89815	0.11471	2.0162
303.126	151.83984	0.07266	2.0082	398.63979	0.11578	2.0084

Just before filling the resonator, we measured the specific conductivity of an aliquot drawn from each sample at 290 Hz with a YSI[4] Model 35 conductance meter. The specific conductivity of samples A, B, and C were 109, 30, and 500 $\mu S \cdot m^{-1}$, respectively, at 23°C.

Each water sample was degassed by boiling for several hours before being inserted into the resonator. Prior to boiling, sample B had also been treated by continuously flowing nitrogen through it for a period of 48 hr. To test that the resonator was free of large bubbles, we measured a resonance frequency at 1, 2, and 3 atmospheres and saw no gross variation in the results. When very small bubbles were present, they could be detected by noting that $\varepsilon'_{high} \neq \varepsilon'_{low}$. (See Section 5.1.)

The resonator was cooled in an ice bath and evacuated. Then, samples were allowed to flow into it under atmospheric pressure. Because the resonator was filled at the lowest temperature of the measurements, the sample expanded out of the resonator as the measurements proceeded from near 0 to 145°C. At the lower temperatures, the measurements of ε_r were made at ambient pressure. Near and above the boiling temperature, the measurements of ε_r were made at least several kilopascals above the saturated vapor pressure. Helium was used to supply this over-pressure. Within the resolution of the measurements of ε_r, the data were independent of pressure. (The pressure derivative $(\partial \varepsilon_r / \partial p)_T = 0.036\ MPa^{-1}$ at 418 K and is smaller at lower temperatures. Thus, we did not expect to detect the pressure dependence of ε_r upon varying the pressure a few hundred kilopascals.)

3.4. Cyclohexane Sample

The cyclohexane was manufactured by Mallinckrodt[4] and is of spectrophotometric ("SpectrAR") grade. The manufacturer's lot analysis specified the purity as 99.0% and the water content as less than 0.02%. No purification was done. Before loading the cyclohexane sample into the resonator, the tubing and valves leading to the resonator were replaced with clean stainless-steel tubing.

3.5. Uncertainties

The predominant sources of error in these measurements of $\varepsilon'(t)$ are the possible dependence of $\varepsilon'(t)$ on residual impurities and the imperfections of our model for the microwave measurements. The polynomial, Eq. (1), was fitted to data for two water samples of substantially different purities and, for each sample, at two substantially different resonance frequencies. Therefore, we take the standard deviation of the data from the least

squares fit as the standard uncertainty for these predominant sources of error.

Two additional uncertainty components result from imperfect temperature and pressure measurements. In practice, these components are almost negligible relative to the standard deviation of the data from Eq. (1); however, these components cannot be evaluated by examination of the data for $\varepsilon'(t)$. Thus, we discuss them now.

The resonator was immersed in a thermostated bath filled with silicone oil. In the bath, the resonator's temperature was controlled to within ± 2 mK. The resonator's temperature was measured with a model F250 digital thermometer manufactured by Automatic Systems Laboratories Inc.[4] The manufacturer claimed that the long term stability was "typically better than 0.005°C per year" and our check of its calibration in 1997 showed that the manufacturer's 1993 calibration was valid. After the measurements of ε_r were completed, the Thermometry Group of NIST compared the readings of this thermometer with standards traceable to ITS-90 at 6 temperatures ranging from 0°C to 140°C. The comparisons extended over several days, and two temperatures were repeated to test for drift. The root-mean-square deviation of the thermometer's reading from the standards' was 0.0062 K. We used twice this value as the measure of the temperature uncertainty. The resulting uncertainty in ε' is 0.0124 K $\times$ $|(\partial\varepsilon'/\partial T)_p|$ which ranges from 0.0051 at 0°C to 0.0026 at 145°C. If these uncertainties are added in quadrature with 0.011 (two standard deviations of the fit to $\varepsilon'(t)$), the resulting overall uncertainty in $\varepsilon'(t)$ is 0.012 at 0°C and 0.011 at 145°C.

The probe of the digital thermometer passed through the stirred bath into a blind hole that had been drilled 8 cm into the center of the upper part of the resonator. Heat-sink paste in the hole was used to increase the thermal conductance between the probe and the resonator.

The pressure was measured with a DH Instruments[4] reference pressure monitor (quartz transducer) that had been calibrated with a piston gage. After calibration, the uncertainty of the pressure measurements was estimated to be 0.04 kPa (2 standard deviations). Because $(\partial\varepsilon'/\partial P)_T$ is small (on the order of 0.04 MPa^{-1} [4]), the data for ε' are not affected by the uncertainties in the pressure measurements.

4. DATA AND RESULTS

4.1. Calibration

The thermal expansion and pressure dilation of the resonator were measured. For this calibration, S_{21} was measured on a series of isotherms

as a function of pressure p when the resonator was filled with helium and with argon. The results with both gases were equivalent. During the same series of measurements, the resonator was also evacuted to determine the temperature dependence of g_α^0. The calibration measurements spanned the ranges $0°C \leqslant t \leqslant 100°C$ and $0 \leqslant p \leqslant 300$ kPa. The data were fitted by functions of the Celsius temperature t of the forms

$$\begin{aligned} f_\alpha &= f_\alpha^0(1+\beta p)/\sqrt{\varepsilon_r} \\ \sqrt{\varepsilon_r} &= 1 + 3A_\varepsilon \rho \\ f_\alpha^0 &= f_\alpha^{00}(1+\alpha_T t) \\ g_\alpha^0 &= g_\alpha^{00}(1+\gamma_T t) \end{aligned} \tag{8}$$

with the values $A_\varepsilon = 4.140\ \text{cm}^3 \cdot \text{mol}^{-1}$ and $A_\varepsilon = 0.5173\ \text{cm}^3 \cdot \text{mol}^{-1}$ for the molar polarizabilities of argon and helium, respectively. A virial equation of state was used to calculate the densities of the gases ρ. The results for the lower frequency mode were: $f_{\text{low}}^{00} = 216.193$ MHz; $g_{\text{low}}^{00} = 0.08570$ MHz; $\alpha_T = -16.8 \times 10^{-6}\ \text{K}^{-1}$; $\gamma_T = 1.49 \times 10^{-3}\ \text{K}^{-1}$; $\beta = 0.12 \times 10^{-6}\ \text{kPa}^{-1}$. The results for the higher frequency mode were: $f_{\text{high}}^{00} = 566.523$ MHz; $g_{\text{high}}^{00} = 0.13469$ MHz; $\alpha_T = -16.4 \times 10^{-6}\ \text{K}^{-1}$; $\gamma_T = 1.40 \times 10^{-3}\ \text{K}^{-1}$; $\beta = 0.13 \times 10^{-6}\ \text{kPa}^{-1}$.

As discussed in Ref. 3, preliminary calibration measurements showed that the half-widths of the resonances were larger than expected from the resistivity of the gold plating and from the losses in the external circuitry. This problem was corrected by applying additional gold plating until the thickness exceeded 30 μm.

4.2. Data for ε'

The "raw" data for the cyclohexane-filled and water-filled resonator are listed in Tables II and III. For each temperature, pressure, and sample, the measured values of f_α and g_α are listed together with computed values of ε'_α. To compute ε'_α, we first corrected the frequencies for the dilation of the resonator with temperature and pressure and also for the term $1/(8Q^2)$ discussed in Section 3.2. Then, the corrected frequencies were substituted into Eq. (6). The values of $(\partial\varepsilon'/\partial P)_T$ reported by Owen et al. in Ref. 4 are of the order of $0.04\ \text{MPa}^{-1}$; thus, the change in ε' from the tabulated pressure of our measurements to the saturated vapor pressure at the same temperature is slightly less than the noise in the present measurements of ε'.

The data for $\varepsilon_i(T)$ were represented by a cubic polynomial function, Eq. (1), and the deviations of the data from this polynomial are shown in

Fig. 2. Considering that the data in Fig. 2 span a factor of 2.6 in frequency and result from two samples spanning a factor of 3.6 in conductivity (at 290 Hz), the residual standard deviation $s = 0.0055$ is remarkably small.

The present results for ε' are compared with data from 11 sources [2, 11–20] in Fig. 1. To avoid clutter in Fig. 1, the baseline is Eq. (1) and a band of width $4s$ indicates the location of the present data. As discussed in the Introduction, the present data are consistent with many previous measurements and are more precise than some. At temperatures below 320 K, there is good agreement between the present data and those from Refs. 2, 14, and 17–19. Above 340 K, the present data are in much better agreement with the transformer-bridge data from Ref. 2 than with the LCR data from Ref. 2. Thus, the present data achieved the goal of discriminating between the two different results obtained in Ref. 2. At temperatures below 320 K, there is clear disagreement between the present data and the very smooth data from Refs. 12 and 15. We cannot explain this disagreement. The same disagreement motivated the measurements in Ref. 2 and was thoroughly discussed there, but not resolved. The reviewers of data from many sources for ε' of water were aware of this disagreement and also have no explanation [7–9].

Figure 4 displays approximations to the derivative $(\partial\varepsilon'/\partial T)_p$ near 100 kPa. Both the solid curve of the upper panel and the baseline of the lower panel are the algebraic derivative of Eq. (1). The points plotted on both panels of Fig. 4 represent the numerical derivative of the data as computed from a linear fit to groups of successive data points spanning intervals of 20 to 30 K. Below 373 K, the data were taken near 100 kPa; thus, the numerical derivative is essentially a constant pressure one. Above 373 K, the data were taken at pressures up to 419 kPa; however, the effect of the difference between the experimental path and a constant pressure path is small compared to the scatter in the numerical derivative of the data.

The residual standard deviation of the points in Fig. 4 from the curves is $0.0018\ \mathrm{K}^{-1}$. The consequences of choosing various algorithms for differentiation are discussed in Ref. 7. There are certainly alternatives (e.g., spline fits) that might result in smaller standard deviations for the derivative.

The lower panel of Fig. 4 also displays $(\partial\varepsilon'/\partial T)_p$ from two recent correlations [7, 8]. Both correlations are in reasonable agreement with the numerical derivative. The second derivative $(\partial^2\varepsilon'/\partial T^2)_p$ plays an important role in solution thermodynamics. Numerical differentiation of Eq. (1) yields the result $d^2\varepsilon'/dT^2 = [1.9175 \times 10^{-3} - 7.9268 \times 10^{-6} t]\ \mathrm{K}^{-2}$. This result is compared with two correlations in Table IV.

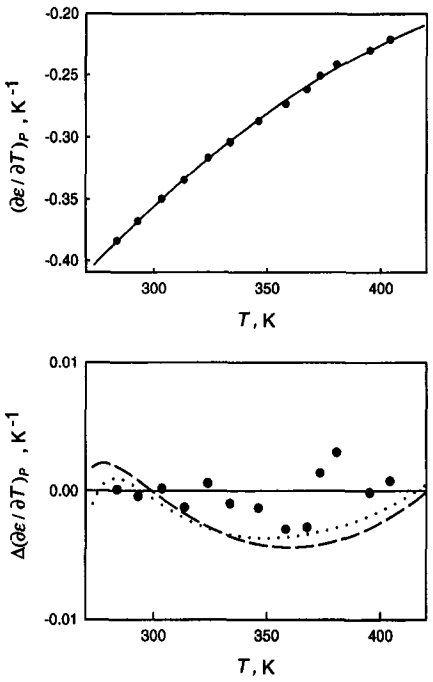

Fig. 4. Top: Temperature dependence of $(\partial\varepsilon'/\partial T)_p$. The solid curve is the temperature derivative of the polynomial function in Eq. (1). The points represent the derivative as computed from linear fits to groups of successive groups of data points spanning intervals of 20 to 30 K. Bottom: $(\partial\varepsilon'/\partial T)_p$ calculated from the data minus the derivative of Eq. (1). The broken curves are correlations: ···, Ref. 8; – – –, Ref. 7.

Table IV. Estimates of $1000 \times (\partial^2\varepsilon'/\partial T^2)_p$ in Units of K^{-2} near 100 kPa

	300 K	350 K	400 K
This work	1.70	1.31	0.91
Ref. 7	1.57	1.28	0.96
Ref. 8	1.58	1.31	0.99

4.3. Conductivity Data

In the present work, $\varepsilon_r = \varepsilon' - i\varepsilon''$ was computed from Eq. (6) and the values of f_α and g_α that had been obtained from fits to the electronically measured quantity S_{21}. Often [10], ε'' is separated into two terms, a "static" electrical conductivity σ and a dielectric relaxation $\varepsilon''_{\text{relax}}$:

$$\varepsilon'' = \varepsilon''_{\text{relax}} + \frac{\sigma}{\omega\varepsilon_0} \tag{9}$$

This decomposition of ε'' is not unique; it depends upon the choice of $\varepsilon''_{\text{relax}}$. For the decomposition, we chose the simple, phenomenological, Debye–Drude model that describes the impedance of water samples over a wide range of conditions. This model has been frequently reproduced [10] and elaborated. In it, the frequency dependencies of ε' and $\varepsilon''_{\text{relax}}$ are

$$\varepsilon' = \varepsilon_\infty + \frac{\varepsilon_s - \varepsilon_\infty}{1 + \omega^2\tau^2} \quad \text{and} \quad \varepsilon''_{\text{relax}} = -\frac{(\varepsilon_s - \varepsilon_\infty)\,\omega\tau}{1 + \omega^2\tau^2} \tag{10}$$

with

$$\tau = 3.77 \times 10^{-15}\ \text{s}\ e^{2300\ \text{K}/T} \tag{11}$$

where T is the kelvin temperature and where we took the value $\varepsilon_\infty = 4$ from Ref. 10. We obtained Eq. (11) for the temperature-dependent relaxation time τ by fitting to the data tabulated in Ref. 9. The relaxation time varies from 18×10^{-12} s near 0°C to 3×10^{-12} s near 75°C and is associated with the reorientation of the dipole moments within the water. At low frequencies, when $\omega\tau \ll 1$, the phenomenological term $\varepsilon''_{\text{relax}}$ is indistinguishable from an electrical conductivity that is proportional to the frequency.

Figure 5 displays the values of σ deduced from the present data and Eqs. (9)–(11). The values of σ spanned a factor of 100 when the sample and the temperature were changed. However, the values of σ deduced from $\varepsilon''_{\text{high}}$ and $\varepsilon''_{\text{low}}$ for a given sample at identical temperatures differed by at most 4% and usually much less. These comparatively small differences confirm the utility of the phenomenological decomposition of ε'', and they are consistent with the assertion that ε_r is measured in the static limit. We recall that the real part of the dielectric constant was nearly the same for samples A and B. (See Figs. 2 and 5.) Thus, an uncertainty of a few percent in the radio-frequency values of σ deduced from the phenomenological decomposition of ε'' does not make an additional contribution to the uncertainty of the dielectric constant.

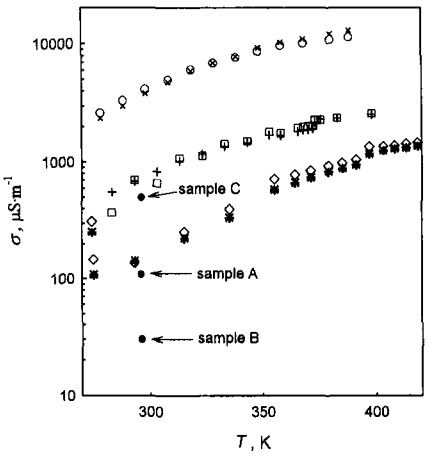

Fig. 5. Temperature dependence of the electrical conductivity of three water samples. The filled points were obtained at 290 Hz with a commercially manufactured conductivity meter. The radio-frequency conductivities were calculated from Eqs. (9)–(11). Key: Sample A, □ f_{low}, + f_{high}; Sample B, * f_{low}, ◇ f_{high}; Sample C, ○ f_{high}, × f_{low}.

Figure 5 also displays the values of σ for each sample that were obtained with a conductivity meter operating at 23°C and 290 Hz. These audio-frequency values of σ are a factor of 4 to 8 smaller than the radio-frequency values obtained at 23°C from ε'' and the Debye–Drude model. We have not attempted to explain this difference because accurate measurements of σ were a byproduct rather than an objective of the present work. We note that a variety of interactions between the electrodes of a capacitor and a conducting dielectric such as water have been described by the term "Maxwell–Wagner effect" [10] and that these interactions can lead to much smaller conductivities at audio frequencies than at radio frequencies. It is also conceivable that the conductivity of the water was increased by contact with some material within the resonator, although the resonator was flushed many times with distilled water prior to loading the samples used here.

4.4. Cyclohexane Data

A limited set of data was taken when the resonator was filled with cyclohexane. These data are listed in Table III in the same format as the

data for water. Our results for ε' of cyclohexane are compared with results from the literature in Table I. As is the case for water, the cyclohexane data are in agreement with data from the literature and the scatter in the present data is smaller than that of the data from the literature.

5. LIMITATIONS OF MEASUREMENTS

5.1. Bubbles

On occasion, while the resonator was filled with water, a bubble (presumably filled with gas that had been dissolved in the sample) spontaneously formed in either the "top" capacitor C_t or the "bottom" capacitor C_b. If the bubble were spherical, one expects that the affected capacitance would be reduced by the factor [10]

$$1 - \frac{3}{2}\frac{(\text{volume of bubble})}{(\text{volume of capacitor})} \tag{12}$$

Even one bubble will reduce both f_{high} and f_{low} and the apparent values of ε' deduced from f_{high} and f_{low} (denoted ε'_{high} and ε'_{low}) because each frequency depends upon both capacitances [3]. The reduction in the apparent values of ε'_{high} and ε'_{low} can be estimated from the circuit parameters in the caption to Fig. 3 together with Eq. (11) of Ref. 3. Theoretically, the reduction in ε'_{low} is 2.9 times larger than the reduction in ε'_{high}. Thus, the presence of a bubble had a characteristic signature; that is, both values of ε' were reduced from the bubble-free values and the reductions were in the ratio 2.9:1. In Table II, there are only three examples of data for Sample A that were influenced by small bubbles ($\sim 1.5\ \text{mm}^3$). These occurred at 273.59, 362.06, and 363.11 K and they were not used in fitting, nor were preliminary data in which larger bubbles reduced ε'_{low} by as much as 0.2. No evidence of bubbles was detected in the data for Samples B and C. Perhaps the treatment of these samples with flowing nitrogen caused this difference. (See Section 3.3.)

5.2. Frequency Dependence

If our understanding of the water-filled re-entrant resonator were perfect, the frequency dependence of ε' displayed in Eqs. (9)–(11) combined with values of τ from the literature would lead to the conclusion: $(\varepsilon'_{low} - \varepsilon'_{high})/\varepsilon'_{low} \leqslant 5 \times 10^{-5}$ and the maximum value of $\varepsilon'_{low} - \varepsilon'_{high}$ would occur near 0°C. This was not the case, as shown for the two purer water samples and for cyclohexane in Fig. 6. We cannot explain why

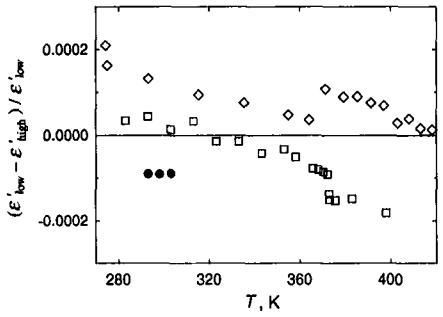

Fig. 6. Dependence of $(\varepsilon'_{low} - \varepsilon'_{high})/\varepsilon'_{low}$ on sample and temperature. Key: □, Sample A; ◇, Sample B; ●, Cyclohexane. The means and the standard deviations of the data sets are: Sample A, $(-0.6 \pm 0.7) \times 10^{-4}$; Sample B, $(+0.8 \pm 0.5) \times 10^{-4}$; Cyclohexane, $(-1.022 \pm 0.005) \times 10^{-4}$.

$(\varepsilon'_{low} - \varepsilon'_{high})/\varepsilon'_{low}$ was as large as 2×10^{-4}. This small dependence of ε' upon the frequency of the measurements is one limitation of the present measurements.

We considered the hypothesis that the unexplained frequency dependence of ε' resulted from a failure of the assumption that the depth of the electromagnetic field's penetration into the gold plating varied as $1/f^{1/2}$; however, the water data and the cyclohexane data have comparable

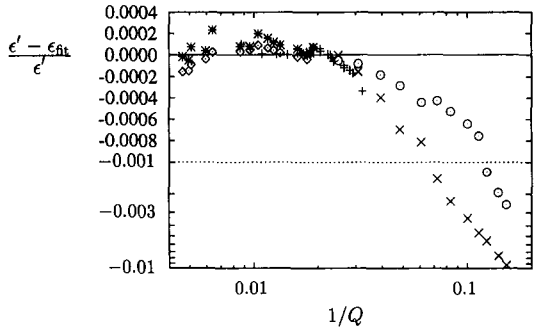

Fig. 7. Fractional deviations of ε' from the polynomial function Eq. (1) as a function of $1/Q$ of the water-filled resonator. The vertical scale is linear from +0.0004 to −0.0010 and logarithmic from −0.0010 to −0.01. Key: Sample A, □ f_{low}, + f_{high}; Sample B, * f_{low}, ◇ f_{high}; Sample C, ○ f_{high}, × f_{low}.

values of $(\varepsilon'_{low} - \varepsilon'_{high})/\varepsilon'_{low}$ although the data span very different frequency intervals. Thus, the explanation must be elsewhere.

5.3. Dependence on the Samples' Conductivity

As the water samples' electrical conductivity increased (particularly by the addition of salt), the Q of the resonator decreased. As shown in Fig. 7, when $1/Q \gtrsim 0.02$, the data deviated systematically from the correlation given by Eq. (1). Under the same conditions, as shown in Fig. 8, the complex Lorentzian function no longer could fit the data for the rf transfer function $\mathbf{S}_{21}$ of the resonator. If one desired to measure ε' of such highly conducting solutions, either the model for the resonator (and the external, measuring circuitry) would have to be improved or the resonator would have to be modified to operate at higher frequencies where the Q was still

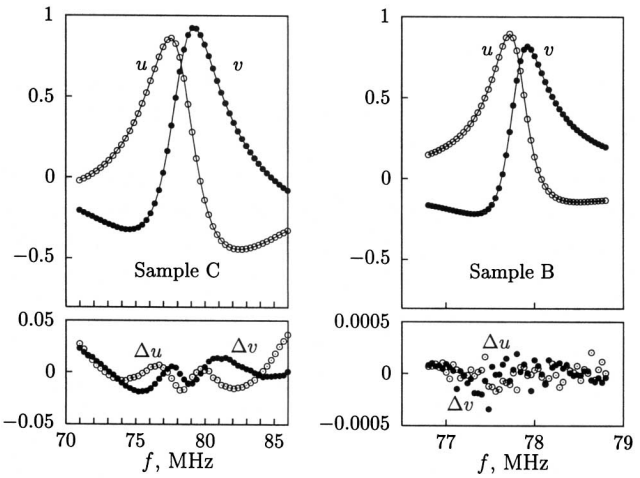

Fig. 8. Complex frequency response ($\mathbf{S}_{12} \equiv u + iv$) of the water-filled resonator. Top: The in-phase (u) and quadrature (v) components of $\mathbf{S}_{12}$ at 385 K. The salted Sample C is on the left; the unsalted Sample B is on the right. Bottom: The deviations ($\Delta u = u - u_{fit}$; $\Delta v = v - v_{fit}$) of the data in the upper panels from Eq. (7). The deviations for the salted sample (lower left) are systematic and large ($s/A_{max} = 0.012$); the deviations for the unsalted sample (lower right) are nearly random and much smaller ($s/A_{max} = 0.00009$). Here s is the standard deviation of the fit to Eq. (7) and A_{max} is the maximum value of the amplitude $(u^2 + v^2)^{1/2}$. Note: the ordinate scale for the lower left is 100 times that of the lower right. The abscissa scale for the lower left is 6.4 times that of the lower right. For Sample C, $Q = 19$; for Sample B, $Q = 165$.

high. The latter approach would fail when the frequency dependence of ε' became substantial.

ACKNOWLEDGMENTS

We thank our colleagues Dr. Daniel Friend, Dr. Dean Ripple, and Dr. Anneke Sengers for their careful reading of the manuscript.

REFERENCES

1. D. P. Fernandez, Y. Mulev, A. R. H. Goodwin, and J. M. H. Levelt Sengers, *J. Phys. Chem. Ref. Data* **24**:33 (1995).
2. D. P. Fernandez, A. R. H. Goodwin, and J. M. H. Levelt Sengers, *Int. J. Thermophys.* **16**:929 (1995).
3. J. Hamelin, J. B. Mehl, and M. R. Moldover, *Rev. Sci. Instruments* **69**:255 (1998).
4. B. B. Owen, R. C. Miller, C. E. Milner, and H. L. Cogan, *J. Phys. Chem.* **65**:2065 (1961).
5. A. R. H. Goodwin, J. B. Mehl, and M. R. Moldover, *Rev. Sci. Instrum.* **67**:4294 (1996).
6. M. R. Moldover, J. B. Mehl, and M. Greenspan, *J. Acoust. Soc. Am.* **79**:253 (1986); J. B. Mehl, *J. Acoust. Soc. Am.* **64**:1523 (1978).
7. D. P. Fernandez, A. R. H. Goodwin, E. W. Lemmon, J. M. H. Levelt Sengers, and R. C. Williams, *J. Phys. Chem. Ref. Data* **26**:1125 (1997).
8. D. G. Archer and P. Wang, *J. Phys. Chem. Ref. Data* **19**:371 (1990).
9. W. J. Ellison, K. Lamkaouchi, and J.-M. Moreau, *J. Mol. Liquids* **68**:171 (1996).
10. J. B. Hasted, *Aqueous Dielectrics* (Chapman and Hall, London, 1973).
11. H. I. Oshry, Ph.D. Thesis (University of Pittsburgh, 1949).
12. C. G. Malmberg and A. A. Maryott, *J. Res. Natl. Bur. Std. (U.S.)* **56**:1 (1956).
13. K. R. Srinivasan, Ph.D. Thesis (Carnegie-Mellon University, Pittsburgh, PA, 1973); K. R. Srinivasan and K. L. Kay, *J. Chem. Phys.* **60**:3645 (1974).
14. C. E. Milner, Ph.D. Thesis (Yale University, New Haven, CT, 1955); H. L. Cogan, Ph.D. Thesis (Yale University, New Haven, CT, 1955).
15. L. A. Dunn and R. H. Stokes, *Trans. Faraday Soc.* **65**:2906 (1969).
16. Yu. M. Lukashov, Ph.D. Thesis (Moscow Power Institute, Moscow, 1981); Yu. M. Lukashov and V. N. Shcherbakov, *Teploenergetica* **27**:171 (1980).
17. G. A. Vidulich and R. L. Kay, *J. Phys. Chem.* **66**:383 (1962); G. A. Vidulich, D. F. Evans, and R. L. Kay, *J. Phys. Chem.* **71**:656 (1967).
18. W. L. Lees, Ph.D. Thesis (Harvard University, Cambridge, MA, 1949).
19. H. Heger, Ph.D. Thesis (University of Karlsruhe, Karlsruhe, 1969); H. Heger, M. Uematsu, and E. U. Franck, *Ber. Bunsenges. Phys. Chem.* **84**:758 (1980).
20. R. Deul and E. U. Franck, *Ber. Bunsenges. Phys. Chem.* **95**:847 (1991).
21. H. T. French, M. Koshla, K. N. Marsh, *J. Chem. Phys.* **20**:1175 (1988).
22. M. Claudius, Diploma work, Meresburg (1975), cited in Landolt-Börstein, Numerical Data and Functional Relationships in Science and Technology, New Series, Editor-in-Chief, O. Madelung, Group IV, Vol. 6 (Springer-Verlag, Berlin, 1991), p. 6–104.
23. U. Credo, Diploma work, Meresburg (1974), cited in Landolt-Börstein, Numerical Data and Functional Relationships in Science and Technology, New Series, Editor-in-Chief, O. Madelung, Group IV, Vol. 6 (Springer-Verlag, Berlin, 1991), p. 6–104.